© 2015
Scienceline Publication
www.science-line.com

ISSN: 2322-5114
Journal of World's Electrical Engineering and Technology
J. World. Elect. Eng. Tech. 4(1): 07-12, April 25, 2015

JWEET

Optimal Design of Bearingless Permanent Magnet-Type Synchronous Motors for Generating Maximum Levitation Force

Mohsen Honarjou, H. Faraji and A. Shirzadi*

Department of Electrical & Avionics Engineering, Malek Ashtar University of Technology, Esfahan, Iran
*Corresponding author's Email: shirzadi_a@yahoo.com

ORIGINAL ARTICLE
PII: S232251141500002-4
Received 07 Sep. 2014
Accepted 25 Oct. 2014

Abstract *– One maintenance task that still exist with conventional motors, are bearing lubrication and renewal. Bearingless motors are replaced with conventional motor that uses a magnetic levitation force to suspend a rotor without any mechanical contact. In bearingless motors, additional windings are wound together with motor windings in stator slots. In this paper, a bearingless permanent magnet-type synchronous motor (BPMSM) Has been studied. First, the generation of radial levitation forces is discussed and then the optimum permanent magnet thickness is determined to produce maximum levitation force. After that the effect of additional winding pole-pair in the amount of levitation force is investigated. The simulation is done in Maxwell software.*

Keywords*: Bearingless Permanent Magnet Synchronous Motor, Maximum Levitation Force, Optimization, Thickness of PM.*

INTRODUCTION

In some applications, bearing maintenance is still a significant problem. For example, the bearings can present a major problem in motor drive applications in outer space, and also in harsh environments with radiation and poisonous substances. In addition, lubrication oil cannot be used in high vacuum, ultra high and low temperature atmospheres and food and pharmacy processes. In these cases magnetic bearing is used. Magnetic bearing is a machine element uses a magnetic levitation force to suspend a rotor. The characteristics of magnetic bearing are no friction, no wear, no lubrication, high speed, high precision, and long operating life. The applications of magnetic bearing are in canned pumps and drives, compact pumps, high-speed flywheel storage system, artificial hearts, Spindle drives and Semi-conductor processing. But magnetic bearing cause long axial length of the rotor shaft and complicated structure and large size of the motor [1-5].

For overcoming these problems, bearingless motors are proposed. Bearingless motor is an electric motor that combines the functions of both torque generation and magnetic suspension together in a single motor. A bearingless motor have two kinds of windings. The conventional windings and suspension winding are wound together in the stator of motor to produce torque and radial suspension force simultaneously. In comparison with magnetic bearing, bearingless motor have Simple structure, higher speed, compactness and lower cost [6-8].

So far, various bearingless motors have been proposed but bearingless permanent magnet synchronous machine (BPMSM) due to its advantages such as simple structure, high efficiency, high torque density, are actively researched and developed around the world. The aim of this paper is to determine the thickness of permanent magnet and to consider the number of suspension windings in order to produce maximum levitation force in BPMSM [9].

MATERIAL AND METHODS

Principles of radial force generation

Figure 1 shows the cross section of a primitive bearingless motor under different conditions. In Figure 1(a), there is a symmetrical 4-pole flux distribution. The solid curves illustrate the flux paths circulating around the four conductors 4a, these conductors are located in the stator slots. The 4-pole flux wave produces airgap poles in the order N, S, N and S in the airgap sections 1, 2, 3 and 4 respectively.

Since the flux distribution is symmetrical, the flux density magnitudes in airgap sections 1, 2, 3 and 4 are of the same value at the same point in the pole section. There are attractive magnetic forces between the rotor poles and stator iron. The amplitudes of these attractive radial forces are the same, but the directions are equally distributed so that the sum of radial force acting on the rotor is zero.

Figure 1(b) shows the principle of radial force generation. Two conductors 2a are located in the stator slots. With the current direction as shown in the figure, a 2-pole flux wave is generated. In airgap section 1, the flux density is increased because the direction of the 4-pole and 2-pole fluxes is the same. However, in airgap section 3, the flux density is decreased because the direction of these fluxes is opposite. The magnetic forces in the airgap sections 1 and 3 are no longer equal, i.e., the force in airgap 1 is larger than in airgap 3. Hence a radial force F

To cite this paper: Honarjou M., Faraji H. and Shirzadi A. 2015. Optimal Design of Bearingless Permanent Magnet-Type Synchronous Motors for Generating Maximum Levitation Force. *J World Elec. Eng. Tech.*, 4 (1): 07-12.
Journal homepages: http://www.jweet.science-line.com/

results in the x-axis direction. It follows that the amplitude of the radial force increases as the current value in conductors 2a increases. Figure 1(c) shows how a negative radial force in the x-axis direction is generated. The current in conductors 2a is reversed so that the flux density in airgap section 1 now decreases while that in airgap section 3 increases. Hence the magnetic force in airgap section 3 is larger than that in airgap section 1, producing a radial force in the negative x-axis direction.

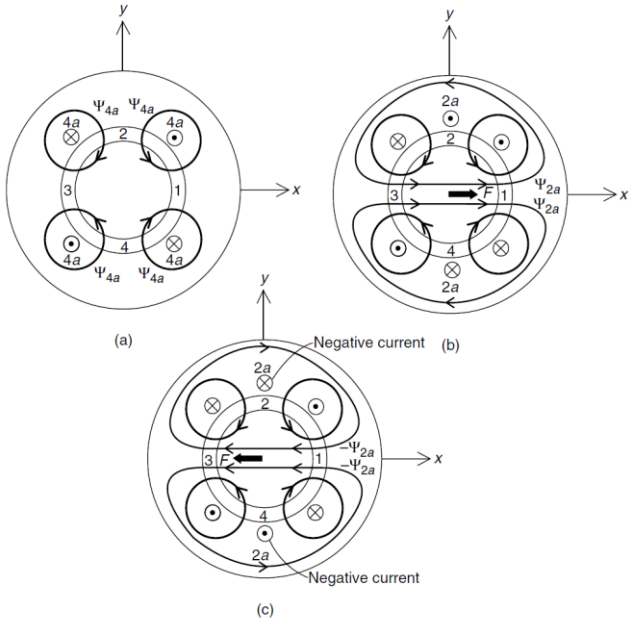

Figure 1. Principles of radial force generation: (a) 4-pole symmetrical flux; (b) x-direction radial force; (c) negative x-direction force [11].

Figure 2 shows radial force generation in the y-axis direction. Two conductors 2b, which have an MMF centred on the y-axis, are added to the stator. A similar flux density imbalance occurs but this time between airgap sections 4 and 2, hence producing a force on the y-axis. The polarity of the current will dictate the direction of the force. These are the principles of radial force generation in x- and y-axis directions. The force values are almost proportional to the current in conductors 2a and 2b (assuming constant 4-pole current). The vector sum of these two perpendicular radial forces can produce a radial force in any desired direction and with any amplitude [11-13].

In order to generate the torque and radial suspension force simultaneously in a bearingless machine the following conditions are

$$\begin{cases} P_M = P_B \pm 1 \\ \omega_M = \omega_B \end{cases} \quad (1)$$

Where and are the pole-pair number and current frequency of the torque winding, and are the pole-pair number and current frequency of the suspension force winding.

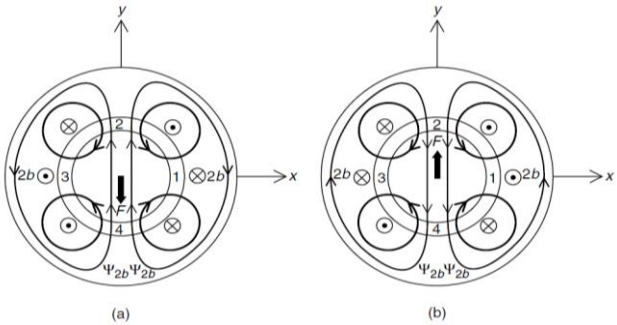

Figure 2. Y-Direction radial force: (a) negative y-direction radial force; (b) y-direction radial force [12].

Figure 3 shows cross-sectional view of a 3-phase bearingless permanent magnet-type synchronous motor. The torque and suspension force windings are wound together in the same stator slots of the BPMSM. Coil sides 4u, 4v and 4w are for the torque windings of phase u, v and w and Coil-sides 2u, 2v and 2w are for suspension force windings of phase u, v and w, respectively. In the figure the torque winding and suspension force winding are 4-pole and 2-pole respectively [14, 15].

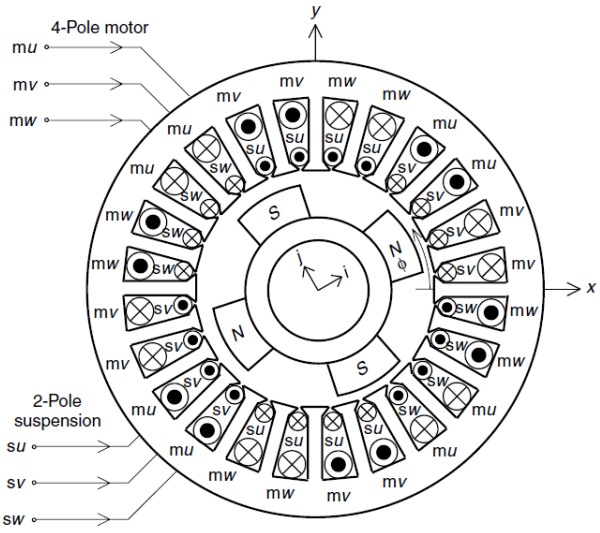

Figure 3. Bearingless permanent magnet bearingless motor [13].

Radial levitation force equation

In this paper, two-phase model of BPMSM is used for simplicity. All of the variables are in the synchronous rotating reference frame.

The relationship between the radial levitation forces and the currents of suspension force winding can be expressed as

$$\begin{cases} F_{ix} = (K_M \pm K_L).(i_{2d}\psi_{1d} + i_{2q}\psi_{1q}) \\ F_{iy} = (K_M \pm K_L).(i_{2q}\psi_{1d} - i_{2d}\psi_{1q}) \end{cases} \quad (2)$$

F_{ix}, F_{iy} are the radial levitation forces. K_M, K_L is Maxwell and Lorentz forces constant. i_{2d}, i_{2q} are current components of radial levitation windings. ψ_{1d}, ψ_{1q} are the airgap flux linkages components of motor windings. The generated Maxwell force F_{sx}, F_{sy} are proportional to the displacement and can be written as

$$\begin{cases} F_{sx} = K_s x \\ F_{sy} = K_s y \end{cases} \quad \text{where} \quad K_s = k\frac{\pi r l B^2}{\mu_0 \delta} \quad (3)$$

Where is the force-displacement Coefficient, is the free space permeability and is the airgap length. So the radial levitation force and can be expressed as

$$\begin{cases} F_x = F_{ix} + F_{sx} \\ F_y = F_{iy} + F_{sy} \end{cases} \quad (4)$$

Substituting (1) , (2) into (3), equation (3) can be written as

$$\begin{cases} F_x = (K_M \pm K_L).(i_{2d}\psi_{1d} + i_{2q}\psi_{1q}) + K_s x \\ F_y = (K_L \pm K_M).(i_{2q}\psi_{1d} - i_{2d}\psi_{1q}) + K_s y \end{cases} \quad (5)$$

When $P_B = P_M + 1$, (4) can be written as

$$\begin{cases} F_x = (K_M + K_L).(i_{2d}\psi_{1d} + i_{2q}\psi_{1q}) + K_s x \\ F_y = (K_L + K_M).(i_{2q}\psi_{1d} - i_{2d}\psi_{1q}) + K_s y \end{cases} \quad (6)$$

When $P_B = P_M - 1$, (4) can be written as

$$\begin{cases} F_x = (K_M - K_L).(i_{2d}\psi_{1d} + i_{2q}\psi_{1q}) + K_s x \\ F_y = (K_L - K_M).(i_{2q}\psi_{1d} - i_{2d}\psi_{1q}) + K_s y \end{cases} \quad (7)$$

The stator flux linkage equation is as follows

$$\begin{cases} \psi_{1d} = L_d i_{1d} + \psi_r \\ \psi_{1q} = L_q i_{1q} \end{cases} \quad (8)$$

Where ψ_r is rotor flux linkages L_d and L_q are the self-inductance of motor Windings [7].

Demagnetization of permanent magnet in BPMSM

In the surface-mounted permanent magnet machines, thin permanent magnets with small airgap can generate the radial levitated forces more effectively. However, thin permanent magnets can simply demagnetize. Thus, it is very important to consider demagnetization of permanent magnets. Moreover irreversible demagnetization of the permanent magnets is a more serious problem in these motors than in conventional electric motors.

Figure 4 shows an example with q-axis motor current and suspension current flux paths. The rotor angular position is 0 deg. When the q-axis motor flux is generated as shown, torque is generated in the counter-clockwise direction. In this case, goes through the permanent magnets denoted as A, B, C and D in the opposite direction to their magnetization. In addition, the suspension flux is shown. Note that both and go through permanent magnet D against the magnetization so that D is the most critical permanent magnet. The q-axis motor flux is synchronously rotating with the rotor but the suspension flux is rotating with a frequency twice that of the rotor, i.e., is not synchronized to the revolving rotor magnetic field. Therefore, not only D but also A, B and C will experience the same degree of demagnetization at some point with the possibility of irreversible demagnetization.

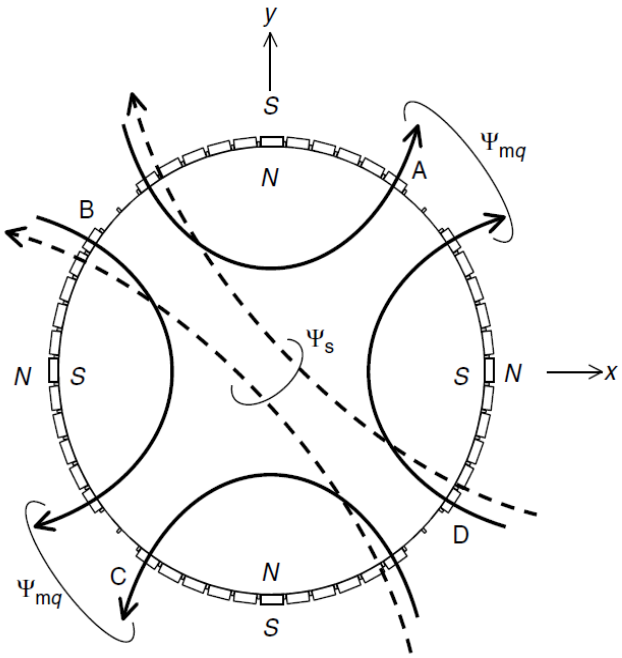

Figure 4. Position of permanent magnet with possibility of irreversible demagnetization [10].

RESULTS

Results and Simulink of model in Maxwell

In this section, FEA is employed to determine the optimum thickness of permanent magnet and number of pole-pair of suspension windings to produce maximum levitation force. The specification of surface-mounted permanent magnet type bearingless motor is shown in Table 1.

Table 1. Specification of BPMSM

Pole pair of torque winding	4
Pole pair of suspension force winding	6
The outer diameter of stator (mm)	155
The inner diameter of stator (mm)	98
The outer diameter of rotor (mm)	88
Axial length of machine (mm)	105
Air-gap length (mm)	4
Residual flux density of PM (NdFeB) (T)	1.28

This motor has 4-pole torque winding and 6-pole suspension force windings. Figure 5 shows the surface mounted permanent magnet bearingless motor in Maxwell software. Since the machine has symmetric flux distribution just one fourth of the machine is sketched in Maxwell software. In the figure, torque and suspension force windings are showed. Mesh diagram produced by finite element analysis is also shown in Figure 6.

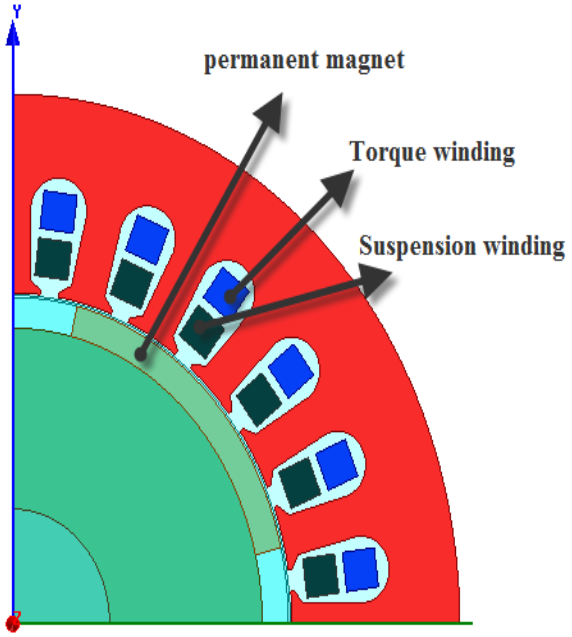

Figure 5. Surface mounted permanent magnet bearingless motor.

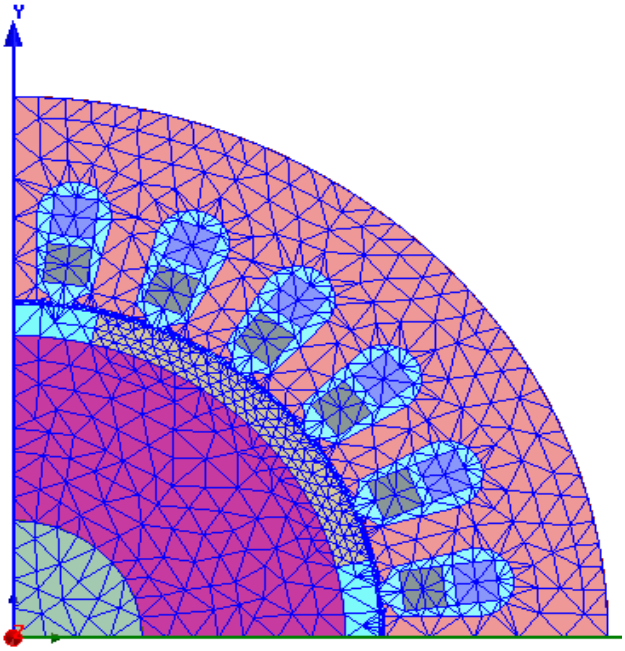

Figure 6. Mesh produced by FEA.

As mentioned earlier, in a permanent magnet motor with fixed airgap length, there is an optimal thickness to generate maximum radial levitation force. The variations of radial levitation force corresponding to the thickness of permanent magnets is analysed in Maxwell software. The results are showen in table (II) and figure 7. In table (II) for different value of PM, the radial levitation force is obtained. It can be seen form figure 7 that levitation force changes corresponding to the thickness of permanent magnets when the length of airgap is fixed. In this paper, the airgap length of motor is 4 mm. As permanent magnet thickness is 1.8 mm, the maximum levitation force is generated (45 N).

Table 2. Thickness of permanent magnet and corresponding levitation force

Thickness of PM (mm)	Radial levitation force (N)
0	0
0.5	9.89
1	28.91
1.5	42.78
1.8	45
2	44.55
2.5	43.25
3	38.23
3.5	35.21
3.8	34.25

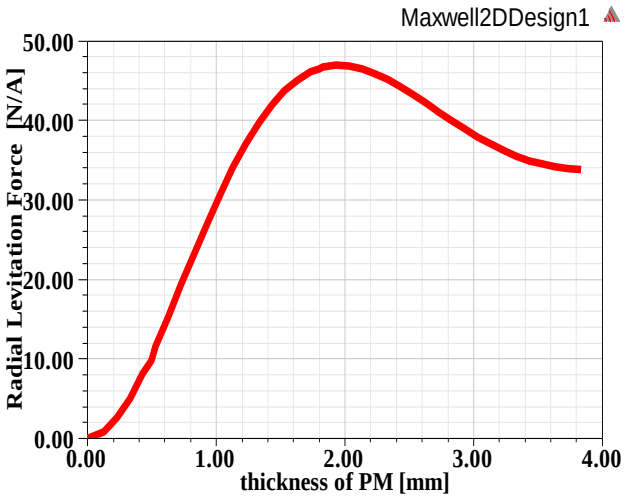

Figure 7. Relationships of radial force and thickness of Permanent magnet.

Now, with this thickness of PM, we must check whether the PM demagnetized or not. Therefore flux density on the surfaces of permanent magnets is derived in Maxwell software and shown in figure 8. It can be seen that the minimum flux density is more than zero, so there is no demagnetization.

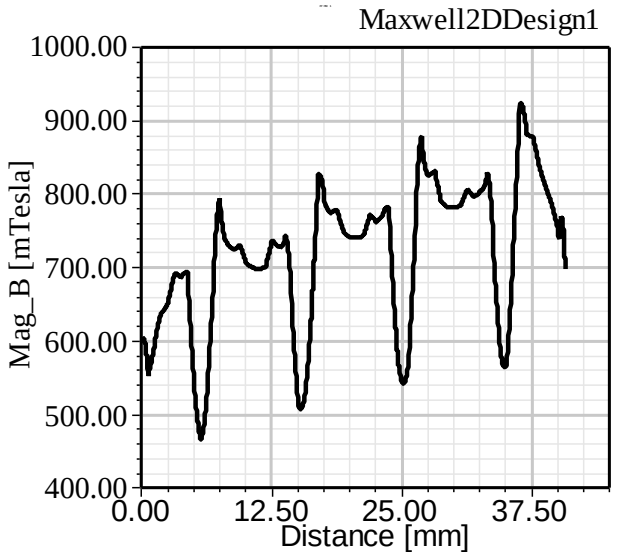

Figure 8. Flux densities on the surfaces of permanent magnet.

In next step, the effect of different pole-pair of suspension winding in the amount of radial levitation force are analyzed. As discussed earlier, for generating levitation force, the number of pole-pair of suspension winding is one more or less than the number of pole-pair of torque windings. So if the pole-pair of torque winding is two, the number of pole-pair of suspension winding is one or three. The effect of different pole-pair of suspension winding in radial levitated force is done in Maxwell software. Results are shown in Figure 9.

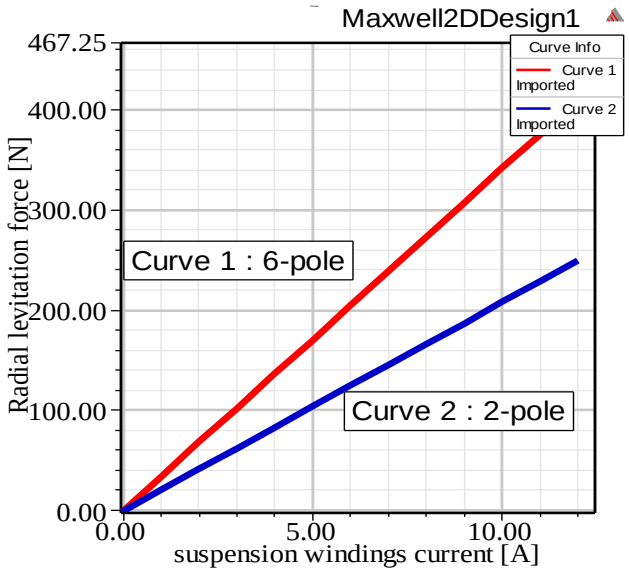

Figure 9. Relationships of the radial levitation force and suspension winding current.

Figure 7 show relation of suspension winding current and radial levitation force with different pole pairs of suspension winding current. Curve 1 of figure 7 shows the relationship between radial levitation forces and 6-pole suspension windings current. Curve 2 of figure 7 shows the relationship between radial levitation force and 2-pole suspension windings current. As shown in Figure 7, it can be seen that radial levitation forces generated by 6-pole suspension windings are larger than that of 2-pole suspension windings under the same pole-pair of torque winding.

CONCLUSION

The aim of this paper is to design a surface mounted permanent magnet-type bearingless motor to produce maximum radial levitation force. First the effect of permanent magnet thickness was evaluated. The optimal permanent magnet thickness is derived 1.8 mm. Second the effect of pole-pair of suspension winding on radial levitation force was evaluated. The result shows that with 6-pole suspension winding the levitation force is greater than that motor with 2-pole suspension winding. So by considering these two notes in design, in addition to increase the radial levitation force, the size of motor is also reduced.

REFERENCES

[1] T. Schuhmann, W. Hofmann, and R. Werner, "Improving operational performance of active magnetic bearings using Kalman filter and state feedback control," IEEE Trans. Ind. Electron., vol. 59, no. 2, pp. 821–829, Feb. 2013.

[2] Y. Ren and J. Fang, "Current-sensing resistor design to include current derivative in PWM H-bridge unipolar switching power amplifiers for magnetic bearings," IEEE Trans. Ind. Electron., vol. 59, no. 12, pp. 4590–4600, Dec. 2012.

[3] J. Fang and Y. Ren, "Self-adaptive phase-lead compensation based on unsymmetrical current sampling resistance network for magnetic bearing switching power amplifiers," IEEE Trans. Ind. Electron., vol. 59, no. 2, pp. 1218–1227, Feb. 2012.

[4] T. Chiba, Fukao, O. Ichikawa, M. Oshima, M. Takemoto, and D. G. Dorrell, Magnetic Bearings and Bearingless Drives. Amsterdam, the Netherlands: Elsevier, Mar. 2005.

[5] T. Reichert, T. Nussbaumer, and J. W. Kolar, "Bearingless 300 W PMSM for bioreactor mixing," IEEE Trans. Ind. Electron., vol. 59, no. 3, pp. 1376–1388, Mar. 2012.

[6] J. Asama, Y. Hamasaki, T. Oiwa, and A. Chiba, "Proposal and analysis of a novel single-drive bearingless motor," IEEE Trans. Ind. Electron., vol. 60, no. 1, pp. 129–138, Jan. 2013.

[7] X. Wang, Q. Zhong, Z. Deng, and S. Yue, "Current-controlled multiphase slice permanent magnetic bearingless motors with open-circuited phases: Fault-tolerant controllability and its verification," IEEE Trans. Ind. Electron., vol. 59, no. 5, pp. 2059–2072, May 2012.

[8] R. Warberger, Kaelin, T. Nussbaumer, and J. W. Kolar, "50 N • m/ 2500 W bearingless motor for high-purity pharmaceutical mixing," IEEE Trans. Ind. Electron., vol. 59, no. 5, pp. 2236–2247, May 2012.

[9] Li and W. Hofmann, "Speed regulation technique of one bearingless 8/6 switched reluctance motor with simpler single winding structure," IEEE Trans. Ind. Electron., vol. 59, no. 6, pp. 2592–2600, Jun. 2012.

[10] H. Grabner, W. Amrhein, S. Silber, and W. Gruber, "Nonlinear feedback control of a bearingless brushless DC motor," IEEE/ASME Trans. Mechatronics, vol. 15, no. 1, pp. 40–47, Feb. 2010.

[11] T. Schneeberger, T. Nussbaumer, and J. W. Kolar, "Magnetically levitated homopolar hollow-shaft motor," IEEE/ASME Trans. Mechatronics, vol. 15, no. 1, pp. 97–107, Feb. 2010.

[12] L. S. Stephens and K. Dae-Gon, "Force and torque characteristics for a slotless Lorentz self-bearing servomotor," IEEE Trans. Magn., vol. 38 ,no. 4, pp. 1764–1773, Jul. 2002.

[13] M. T. Bartholet, T. Nussbaumer, and J.W. Kolar, "Comparison of voltagesource inverter topologies for two-phase bearingless slice motors," IEEE Trans. Ind. Electron., vol. 58, no. 5, pp. 1921–1925, May 2011.

[14] N. Quang Dich and S. Ueno, "Analysis and control of nonsalient permanent magnet axial gap self-bearing motor," IEEE Trans. Ind. Electron., vol. 58, no. 7, pp. 2644–2652, Jul. 2011.

[15] F. Rodriguez and J. A. Santisteban, "An improved control system for a split winding bearingless induction motor," IEEE Trans. Ind. Electron., vol. 58, no. 8, pp. 3401–3408, Aug. 2011.